STALL CONTROL ON THE NACA 23012 AIRFOIL VIA SINGLE AND DOUBLE SUCTION

Alonge, O. I.[1*], Akinneye, A.O. [1] and Julius, M. O. [2]

[1] Department of Mechanical Engineering, Elizade University, Ilara-Mokin, Ondo State, Nigeria.

[2] Department of Mechanical Engineering, Obafemi Awolowo University, Ile-Ife, Osun State, Nigeria.

* Email of Corresponding Author: alongeoluwasanmi@gmail.com

ABSTRACT

Flow separation due to adverse pressure gradients is the driving agent for the stalling of wings and consequently aircraft which may lead to disaster. Therefore, this paper focuses on the control of the negative effects of stall on the aerodynamic performance of a NACA 23012 airfoil through the implementation of suction on the upper surface of the airfoil. The suction is carried out at a Reynolds number of $Re = 6 \times 10^6$, at angles of attack from 0º to the critical angle. Considering the suction position, and the suction width for a single suction, the capability of suction to control stall is studied. Also, double suction was implemented to determine the effect of multiple slots. The numerical analysis was carried out using the Reynolds Averaged Navier-Stokes equations (RANS) in conjunction with the k-omega (SST) turbulent model. The results from this investigation show that suction is more effective closer to the leading edge by boosting lift by as much as 25% and reducing drag by over 70%. The use of double suction offered no improvements over single suction other than extending the critical angle of attack to 28 º.

Keywords: flow control, airfoil, suction, boundary layer separation

NOMENCLATURE

α	airfoil angle of attack
α_{stall}	stalling angle of attack, coincident with the maximum lift coefficient
c	airfoil chord length drag coefficient
C_μ	suction coefficient
H	dimensionless jet width
C_d	drag coefficient

C_L	lift coefficient
AOA	angle of attack
x/c	separation position
Re	Reynolds number based on chord surface length along with airfoil profile
L_j	suction width
Λ	suction jet amplitude
L_p	suction position
ρ	the density of the fluid
N	number of element
$\bar{P}$	the mean pressure
v	the kinematic viscosity
u_{jet}	the suction jet velocity
u_∞	the free stream velocity
$\bar{u}$	the mean velocity
$\overline{u_i' u_j'}$	the Reynolds stress tensor
F_1	the blending function
S	the invariant measure of the strain rate
P_∞	mainstream static pressure
P_c	local static pressure of the slot
C_{d_s}	equivalent suction drag coefficient
$C_{d\_baseline}$	drag coefficient without suction
$C_{d\_suction}$	drag coefficient with suction

INTRODUCTION

Stall is a direct consequence of airflow separating from the surface of lift generating bodies such as airfoils (Anderson, 1987). Airflow separates due to the adverse pressure gradients which occur in the boundary layer of airfoils. Stalling reduces the lift force that keeps the airfoil airborne while simultaneously increasing the drag force that slows the airfoil, which decreases the lift even more (White, 2011). The balance of pressure forces acting on the rear and front surfaces of the airfoil is crucial to the onset of flow separation as an imbalance would cause flow separation (Anderson, 2011). The combination of the adverse pressure gradient and skin friction forces at high angles of attack give rise to poor aerodynamic performance of aircrafts and drones alike. There have been various investigations which have been carried out in the past with regards to how separation of airflow can be controlled. Loftin and Smith (1948) experimentally studied the aerodynamic characteristics of NACA 23012 wing under various aerodynamic conditions with trailing edge flaps and at varying Reynolds numbers from

7×10^5 *to* 6×10^6. They concluded that NACA 23012 has very good aerodynamic characteristics. Zha et al., (2007) developed novel control methods which involve the use of a co-flow jet (CFJ) on the top surface of the airfoil. The co-flow jet consists of an injection slot where high velocity air is fed to supplement the external air and increase the overall kinetic energy of the flow on the airfoil top surface. A suction slot is also present at the trailing edge which sucks the air in. The results from this setup show enhanced lift and increased stall margin. The CFJ differs from other circulation techniques which rely on larger leading or trailing edges to utilize the Coanda effect and enhance circulation. Kirk (2009) used both experimental and computational methods to evaluate a NACA 6415 airfoil. Analysis was carried out on the enhanced model of the airfoil which possessed injection and suction slots on the top surface of the airfoil. The results of the wind-tunnel experimentation and the computational simulation showed an improvement in the aerodynamic performance of the airfoil when the suction and injection was employed. Azim et al., (2015) carried out numerical analysis on the NACA 4412 airfoil to determine its aerodynamic characteristics and aimed to delay flow separation via suction alone. The suction slot with a width of 2% of the chord was moved across the length of the chord to find the best position to achieve the best results. It was observed that suction at the 0.68 c position for a constant AoA=120º and M=0.6, moves the separation position to 0.96c of the airfoil. Also, suction with 65kPa makes lift to drag ratio 35% higher than that of suction at 80kPa. Yousefi et al., (2014) carried out CFD analysis to determine the effects of jet width on blowing and suction flow control for a NACA 0012 airfoil. Tangential and perpendicular blowing methods were employed via suction slots which varied from 1.5 % to 4% of the chord length with the jet velocity at the slots set at half of the free stream velocity. By employing the suction control flow technique, the lift coefficient increased by approximately 75% and the drag coefficient decreased by 56%. The most effective jet widths for achieving all desirable effects are 2.5% to 3% of the chord length for suction at the airfoil leading edge. Huang *et al*., 2004 numerically investigated blowing and suction on the NACA 0012 airfoil, with a jet width of 0.025c. The physical mechanisms that govern suction and blowing flow control were determined and analyzed, and the critical values of suction and blowing locations, amplitudes, and angles were discussed. They concluded that suction created a larger and lower pressure zone than blowing and was more effective at the leading edge and that blowing was very effective further downstream of the airfoil surface. Chen et al., (2014) experimentally worked on the suppression of vortex shedding on a circular cylinder via the suction flow control method. They concluded that the suction control method excellently

suppressed the alternative vortex shedding from the circular cylinder model and the fluctuations of the lift coefficients and drag coefficients of the cylinder model were reduced intensely. Carnarius et al., (2004) numerically investigated the steady flow field around a NACA 4412 at Reynolds number$= 10^6$. They concluded that separation was successfully controlled by steady suction upstream of the separation and when the suction angle was varied from $\beta = 20^o$ to $\beta = 160^o$, it was found that suction perpendicular to the slot surface was optimal. Atik and Walker (2005) worked on a series of numerical simulations to explore the effect of suction and suction/blowing as control mechanisms of leading-edge separation at high Reynolds number. They revealed that a single suction control has better suppression effects than the blow/suction control. The investigations have shown that suction located at an appropriate position modifies pressure distribution over an airfoil surface as such produce a satisfactory effect on lift and drag coefficients, hence mitigating the streamwise momentum loss in the growth of the separation thickness. In the current study, the effects of main parameters of suction control, such as suction location, coefficient, and slot size, on flow separation and aerodynamic performance of a NACA23012 aerofoil is numerically analysed at Reynolds number 6×10^6.

METHODOLOGY

The geometry of a NACA 23012 aerofoil, suction jet location, suction jet angle and the jet length are shown in Figure 1. The chord length of the aerofoil was 1*m*; the suction jet length for this investigation was 2% of the chord length (Yousefi, 2014) and the suction jet amplitude (Λ) which is the ratio of the suction jet velocity to free stream velocity) was 0.5. The fluid was modelled as a two dimensional, steady, turbulent and viscous incompressible flow with constant temperature and ambient pressure. The equations which govern the motion of fluids are the Navier-Stokes equations.

$$\frac{\partial \overline{u_i}}{\partial x_i} = 0 \qquad (1)$$

$$\frac{\partial (\overline{u_i u_j})}{\partial x_j} = -\frac{1}{\rho}\frac{\partial \bar{P}}{\partial x_i} + \frac{\partial}{\partial x_j}\left[\nu \frac{\partial \overline{u_i}}{\partial x_j} - \overline{u_i' u_j'}\right] \qquad (2)$$

where $\overline{u_i' u_j'}$ is the Reynolds stress tensor that incorporates the effects of turbulence (Alfonsi, 2009).

Turbulence models are mathematical equations which predict turbulence and its accompanying effects in fluid flows. Due to the closure problem presented by the fluctuations of velocity in the RANS Equations, turbulence models are needed to close the equations and only obtain mean values of velocity and pressure (Alfonsi, 2009). The turbulence model used in this project is the Menter $k-\omega$ two-equation model which incorporates Shear stress transport modelling. This turbulence model is excellent in its ability to predict flow separation; a critical characteristic necessary for the sake of accuracy in this project. The model has the ability to switch between the $k-\varepsilon$ and $k-\omega$ models when considering the flow away from the surface to the boundary layer (Menter, 1994). The equations are expressed as;

$$\frac{\partial}{\partial x_i}(\rho U_i k) = \widetilde{P_k} - \beta^* \rho k\omega + \frac{\partial}{\partial x_i}\left[(\mu + \sigma_k \mu_t)\frac{\partial k}{\partial x_i}\right] \qquad (3)$$

$$\frac{\partial}{\partial x_i}(\rho U_i \omega) = \alpha\rho S^2 - \beta\rho\omega^2 + \frac{\partial}{\partial x_i}\left[(\mu + \sigma_\omega \mu_t)\frac{\partial \omega}{\partial x_i}\right] + 2(1-F_1)\rho\sigma_{\omega 2}\frac{1}{\omega}\frac{\partial k}{\partial x_i}\frac{\partial \omega}{\partial x_i} \qquad (4)$$

where β^* is 0.09 and $\sigma_{\omega 2}$ is 0.856. $\widetilde{P_k}$, a production limiter, was used in the SST model to prevent the build-up of turbulence in the stagnation regions (Menter, 1992 and Menter, 2003). This research was carried out using ANSYS FLUENT. Values for the Reynolds number and the free stream velocity were $6 \times 10^6$and 85.242 *m/s* respectively. The second-order upwind scheme was employed to discretize the governing equations. In the simulations, second-order upwind discretization in space was used and then, the resulting system of equations was solved through Semi-Implicit Method For Pressure Linked Equations (SIMPLE) procedure until a convergence criterion of reduction in all dependent residuals was satisfied (Kirk, 2009). A C-type structured grid was generated as a computational domain as shown in Figure 2. The computational area was large enough to ensure that there were no interactions between the flow close to and around the airfoil and the outer domains. The total length of the flow domain was set at 10 chord lengths (10c) and the diameter of the flow domain front arc was 10 chord lengths as well. The arc, upper, and lower boundaries of the flow domain were set as an inlet and prescribed a uniform velocity boundary condition of 85.242 m/s. The back of the flow domain was prescribed as an outlet boundary condition with constant atmospheric pressure of 101.325 kPa. No slip boundary condition was used on the airfoil surface. A low free-stream turbulence intensity of 0.01% was used to match the characteristics of a wind tunnel with finely straightened air flow or typical external airflow where the air is initially still and the mesh of $y^+<1$ around the airfoil/ wing was ensured to ensure the viscous effects around the boundary

layer were properly captured by the simulation and for the turbulence model to work effectively.

The computations of variable density meshes were performed for the NACA 23012 aerofoil at Reynolds number 1×10^6 to ensure mesh independence test to the calculated results through the analysis of the lift and drag coefficients at angle of attacks of 4º, and 14º for a baseline airflow over the airfoil without the use of suction on the aerofoil surface as shown in Table 1. From Table 1, the mesh size with the fine mesh following a grid independent result that produces a reasonable accuracy was selected to be 111,560 cells where lift and drag ceased to have significant change as the number of elements increased. For the validation of the data, the residuals in all simulations were continuing until the lift and drag coefficients converged. The lift and drag coefficient were studied and compared with the experimental values of Loftin and Smith (1945), the variation in values between the experimental and CFD results can be attributed to factors such as choice of Turbulent model, the airfoil geometry (particularly the asperities present in physical models) and the sensitivity or calibration of the equipment used for the experiments. The suction jet location (L_j) was investigated for optimum performance of the NACA 23012 wing, once the best position for suction was determined; a second slot was placed with the same jet width of 0.02c and a spacing of 0.01c to test the effects of multiple suction slots on airfoil performance. The suction spacing was chosen so as to not only minimize interaction between the two slots but also ensure the slots were not placed too far apart and could not be considered as being in the same position which gave the best results from the single suction simulations. Since stall occurs on NACA 23012 at around 18º AOA, and flow separation begins around 10º, the single slot investigations were carried out between 0º – 18º angles of attack. The jet entrance velocity components are defined using Eq. 5 and 6:

$$u_j = V_\infty \Lambda \cos(\beta + \theta) \quad (5)$$

$$v_j = V_\infty \Lambda \, sin \, (\beta + \theta) \quad (6)$$

θ represents the angle of flow entrance irrespective of slot position (-90 degrees in the case of suction) and β is the angle between the free-stream velocity direction and the local jet surface

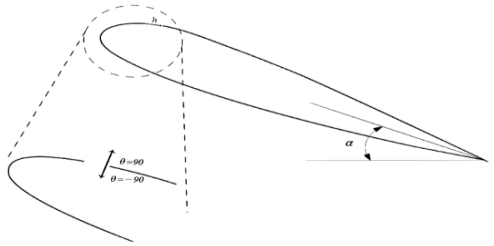

Figure 1: design of the suction mechanism on NACA 23012 with suction parameters.

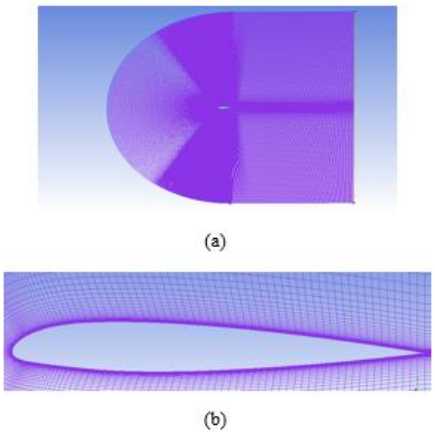

Figure 2: Structured Mesh of a NACA 23012 Aerofoil (a) full view of mesh (b) close-up view of mesh close to airfoil.

Table 1: Mesh Independence Study at Angle of Attack (AOA) of 4^0 and 14^0

	4 ° AOA		14 ° AOA	
No. of cells	**C_L**	**C_D**	**C_L**	**C_D**
20,960	0.54320	0.0129	1.409	0.034
39,860	0.54176848	0.012873387	1.4164643	0.033025406
59,760	0.54147471	0.012845724	1.4164998	0.032525105
83,660	0.53850916	0.012789595	1.4075339	0.032657886
111,560	0.53845817	0.012813948	1.4187399	0.032496861
143,460	0.53843519	0.012840244	1.4177279	0.032590479

RESULTS AND DISCUSSIONS

Flow characteristics without suction

The suction amplitude is used to quantify the energy control consumption as expressed in Equation 9.

$$C_\mu = \frac{\rho \times h \times u_j^2}{\rho \times C \times u_\infty^2} = \frac{h}{C} \times \frac{u_j^2}{u_\infty^2} \quad (7)$$

$$H = \frac{h}{C} \quad (8)$$

$$C_\mu = H \times \Lambda^2 \quad (9)$$

The mesh structure of the suction slot is shown in Figure 3. The first slot was located at 0.05c and moved further downstream to 0.50c and 0.95c. The redesigned airfoil makes use of suction to create a low pressure (relative to the ambient pressure) environment. This causes the air to flow towards the low-pressure region in an attempt to balance the pressure. Ultimately, the suction induced high kinetic energy into the boundary layer flow.

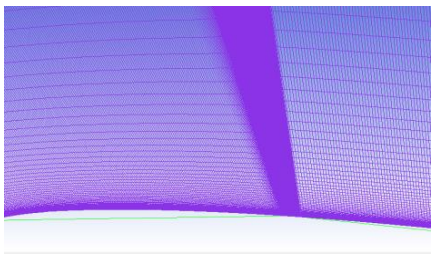

Figure 3: Dense meshes around the suction slot

Figure 4 shows the Comparison between lift coefficient of present work and experimental work by Lofin and Smith (1949) while Figure 5 illustrates the changes in the velocity distribution over the airfoil as it increases its angle of attack. At 6 deg., the flow separation is minimal, as the angle of attack increases, the lift equally increases and the flow separation begins to move further upstream of the airfoil, hence the progressively increased deep blue regions of low velocity going from Figure 5 (a-d). In Figure 5(d) the flow has completely separated from the

airfoil and the lift begins to drop. This is the critical angle of attack of the airfoil, and is the angle wherein the airfoil generates maximum lift. Also, the drag increases as the angle of attack increases due to the increase in pressure drag brought about by flow separation.

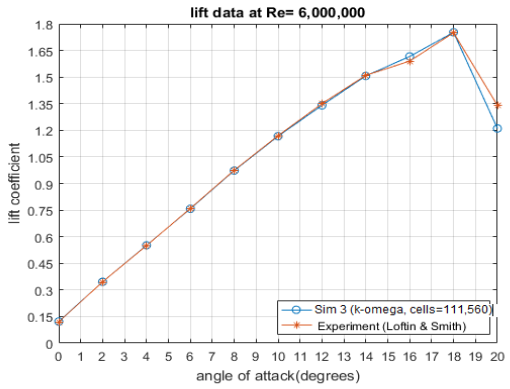

Figure 4: Comparison between lift coefficient of present numerical work, and experimental results by Loftin and Smith.

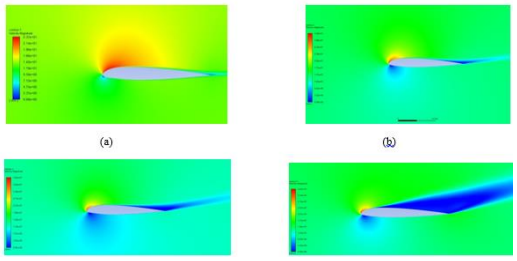

Figure 5: Velocity distribution around the airfoil for single suction at angle of attack (a) 6^o (b) 12^o (c) 15^o (d) 18

Stall Control using Single Suction

The control of the stall of the NACA 23012 airfoil through suction is dependent on the optimised suction parameter used. The suction width is taken as 0.02c and the slots were placed in three locations on the airfoil top surface at 0.05c, 0.50c and 0.95c. Figure 6 shows the velocity contours ranging from no suction to the suction occurring at various positions on the airfoil upper surface at $Re = 6 \times 10^6$ and $\propto = 16°$. The flow separation is controlled as the thickness of the high pressure (very low velocity) region representing separation region are smaller, for the suction at 0.05 and 0.50c, however at 0.95c the suction is not effective and produces a similar velocity profile about the airfoil as the case of no suction. Figure 7 and 8 show the variations in drag coefficient and lift coefficient. As the suction slot moves further downstream, the drag coefficient increases. The drag coefficient is the sum of pressure drag

coefficient and friction drag coefficient (Anderson, 1987), here, the pressure drag is dominant. However, the decrease in drag coefficient was due to a large decrease in the pressure drag coefficient gradient. However, as previously observed in Figure 8, the drag experiences an increase for the slot at 0.95c. This can be attributed to the build-up of the skin friction drag as the air travels over the airfoil surface. The maximum lift coefficient C_l increases with the use of suction as well and the critical angle is extended. Lift coefficient C_l increases only when the flow separation has been reduced which has occurred in this case via the increase in momentum of the fluid through suction or the greater pressure difference between the upper and lower surfaces brought about by the lower (relative to ambient, P_∞) suction pressure (P_s). Although, per angle of attack, the suction at 0.95c produces greater lift it has a lower critical angle of attack and lower maximum lift coefficient than the slots placed further upstream. Fig. 9(a) and (b) shows the variation of lift and drag coefficient with suction and without suction at different angle of attack. For the slot at 0.05c, the use of suction at the leading edge gave better combined lift and drag coefficient results than the slots placed further downstream. The maximum lift coefficient is increased by 25% while the critical angle of attack is 24º. The effects of the suction are more pronounced at angles of attack above 14º. The drag coefficient drastically reduces at higher angles of attack, at an angle of attack of 20º; the drag is reduced by 72%. While remaining relatively similar to the values of the baseline airfoil at angles of attack below 10º.

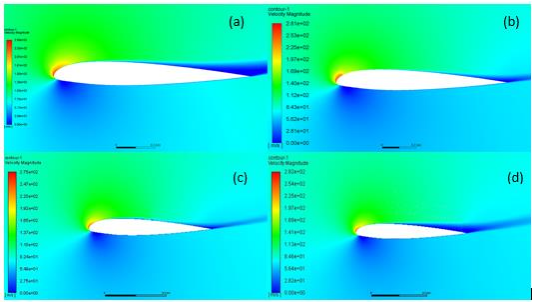

Figure 6: Velocity contours for single suction at AoA =16º for (a) Baseline (top left) (b) slot at 0.05c (top right) (c) 0.50c (bottom left) (d) 0.95c (bottom right)

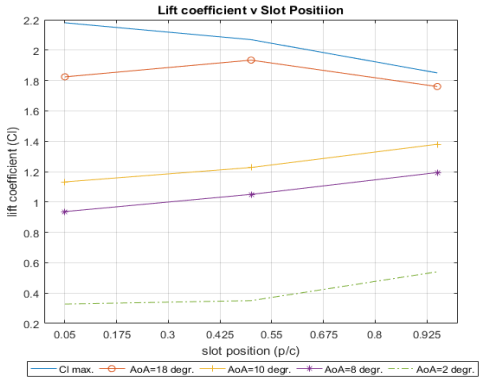

Figure 7: Lift coefficient values for different Angles of attack (AoA) for different slot positions

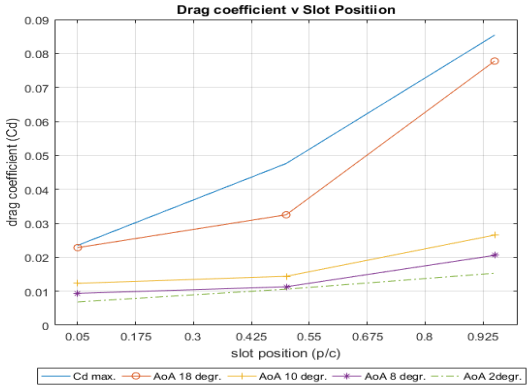

Figure 8: Drag coefficient values for different Angles of attack (AoA) for different slot positions

Stall control using double Suction

The best position for suction based on the simulations conducted with single suction was at 0.05c. At this position two slots were placed to determine the effect of double slots on flow separation and ultimately airfoil aerodynamic performance. The two slots have a slot width of 0.02c and were separated by a distance of 0.01c. The Suction jet amplitude 0.5 was used and the Reynolds number of the flow was kept at 6,000,000. Figure 10 and 11 show the lift and drag coefficient while Figure 12 (a&b) shows the static pressure and velocity contour at different angle of attack. Figure 13 & 14 show the lift and drag coefficient values for all conditions. The double-slot does not increase the maximum lift coefficient, although it increases the critical stall angle to 28º. The Drag coefficient, although lower in the case of the double-slot, offered no improvements to the single-slot case, rather it produced more drag than a single slot at the same position (0.05c). The double slot produced a fairly similar drag profile to the case of no suction for angles of attack below 10º.

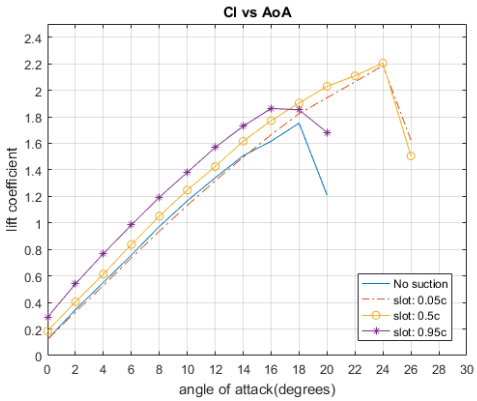

(a)

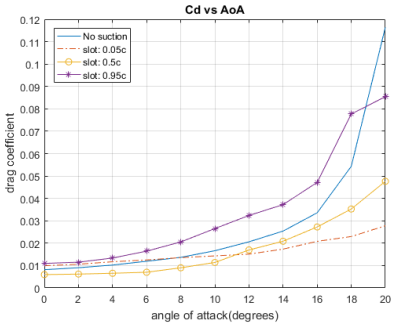

(b)

Figure 9: Variations of (a) lift coefficient and (b) drag coefficient with angle of attack without and with suction conditions

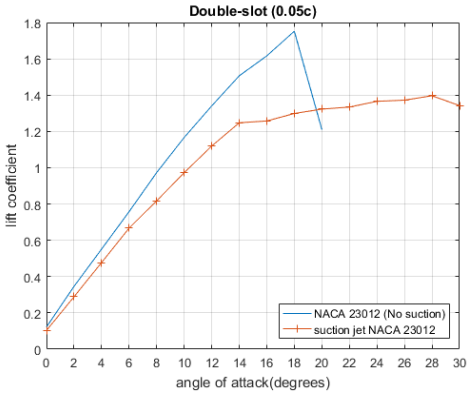

Figure 10: Lift coefficient values for double-slot at 0.05c

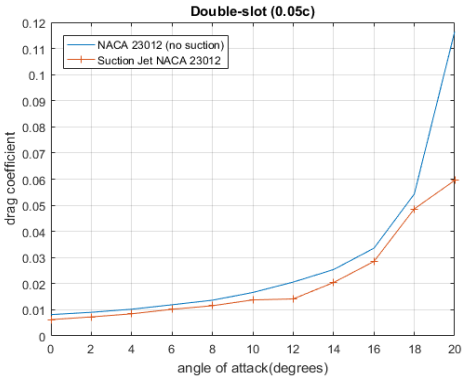

Figure 11: Drag coefficient values for double-slot at 0.05c

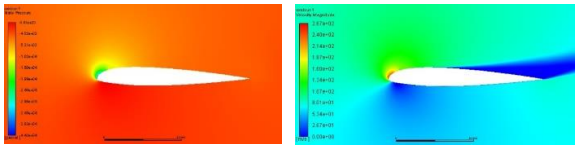

(a) (b)

Figure 12: (a) Static pressure and (b) velocity pressure at AoA=16 for double slot

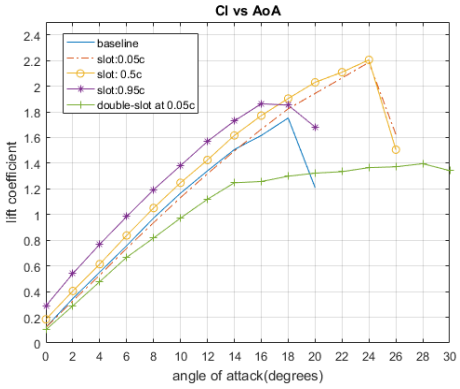

Figure 13: Lift coefficient values for all flow conditions

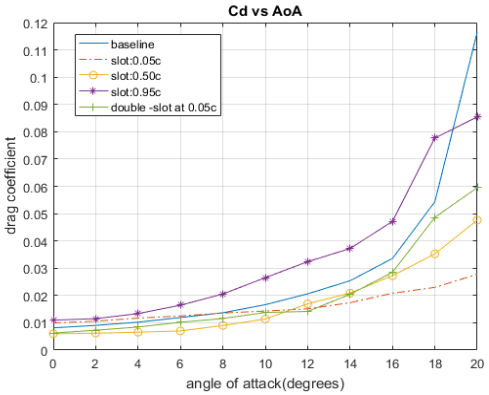

Figure 14: Drag coefficient values for all flow conditions

CONCLUSION

Suction increased the lift on the airfoil and simultaneously reduced the drag on the airfoil by inducing higher energy flow that helped the fluid to traverse the adverse pressure gradients. The suction also created a lower pressure region on the upper surface of the airfoil which created a larger pressure difference necessary for increasing lift. The suction slot close to the leading edge (0.05c) gave the best results, although the suction slots at the downstream slots gave higher lift values per angle of attack. The drag was higher for these downstream slots and for the slot at 0.95c the airfoil stalled at a lower angle of attack than the baseline airfoil. From this investigation, doubling of the suction slot at the best suction position (0.05c) did not reduce flow separation although it extended the critical angle of attack. It however offered no advantages to the single slot suction at that same position.

REFERENCES

Alfonsi, G., 2009. Reynolds-Averaged Navier–Stokes Equations for Turbulence Modeling, Jounal of Applied Mechanics, 62, 4, 040802.

Anderson, J. D., 1987. Introduction to flight. McGraw-Hill Education.

Anderson, J. D., 2011. Fundamentals of aerodynamics. McGraw-Hill Education.

Atik, H., and Walker, D., 2005. Boundary-layer Separation Control Using Local Suction and Injection. In 4th AIAA Theoretical Fluid Mechanics Meeting , 4937.

Azim, R., Hasan, M. M., and Ali, M., 2015. Numerical investigation on the delay of boundary layer separation by suction for NACA 4412, Procedia Engineering, 105, 329-334.

Carnarius A, Bert G., Wachsmuth D. F. Tr, and. Reyes J. C. D. L, (2004). Numerical Study of the Optimization of Separation Control, American Instituite of Aeronautics and Astronautics, pp. 1–17.

Chen, W., Liu, Y., Xu, F., Li, H., and Hu, H., 2014. Suppression of vortex shedding from a circular cylinder by using a traveling wave wall, In 52nd Aerospace sciences meeting (p. 0399).

Huang, L., Huang, P. G., LeBeau, R. P., and Hauser, T., 2004. Numerical study of blowing and suction control mechanism on NACA0012 airfoil, Journal of aircraft, 41(5), 1005-1013.

Kirk, D., 2009. Experimental and Numerical Investigations of a High Performance Co-Flow Jet Airfoil, A Masters thesis.

Loftin Jr, L. K., and Smith, H. A., 1945.

Aerodynamic Characteristics of Fifteen NACA Airfoil Sections at Seven Reynolds Numbers from 0.7×10^6 to 9×10^6, NAtional Advisory Committee of Aeronautic, Technical Report Note.

Menter, F. R., 1994. Two-equation eddy-viscosity turbulence models for engineering applications, AIAA Journal 32,8, 1598-1605.

Menter, F. R., 1992. Improved Two-Equation Turbulence Models for Aerodynamic Flows," Moffett Field.

Menter, F., Kuntz, M., and Langtry, R., 2003. Ten Years of Industrial Experience with the SST Turbulence Model, Turbulence Heat and Mass Transfer, 4, 625–632.

White, F. M., 2011. Fluid Mechanics, New-York, MacGraw-Hill.

Yousefi, K., Saleh, R., and Zahedi, P., 2014. Numerical study of blowing and suction slot geometry optimization on NACA 0012 airfoil. Journal of Mechanical Science and Technology, 28(4), 1297-1310.

Zha, G., Gao, W., and Paxton, C. D., 2007. Jet effects on coflow jet airfoil performance. American Institute of Aeronautics and Astronautics Journal, 45(6), 1222-1231.